Electronic supplementary information

In-situ grown Nickel Nanoparticles in Calixarene Nanoreactor on Graphene-MoS_2 Support for Efficient Water Electrolysis

Babasaheb J. Waghmode*[ab], Siddheshwar N. Bhange[c], Sreekuttan M. Unni[d], Kashinath R. Patil[b] and Dipalee D. Malkhede*[a]

[a]Centre for Advanced studies in Chemistry, Department of Chemistry, Savitribai Phule Pune University, Pune-411007, India.

[b]Centre for Materials Characterization Division, CSIR-National Chemical Laboratory, Dr. Homi Bhabha Road, Pune- 411008, India.

[c]Physical and Materials Chemistry Division, CSIR-National Chemical Laboratory, Dr. Homi Bhabha Road, Pune-411008, India.

[d]Laboratory for Chemistry and Life Sciences, Tokyo Institute of Technology, R1-17, 4259 Nagatsuta, Midori-ku, Yokohama 226-850, Japan.

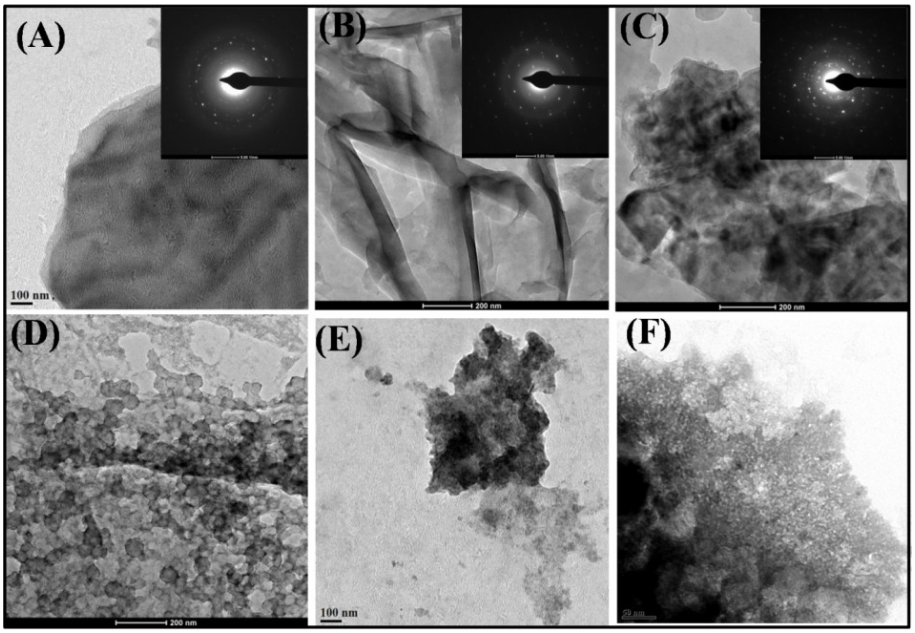

Figure S1. TEM micrograph of (A) Gr (B) MoS_2, (C) Gr-MoS_2, (D) Ni, (E) GrSC8Ni and (F) MoS_2SC8Ni electrocatalysts.

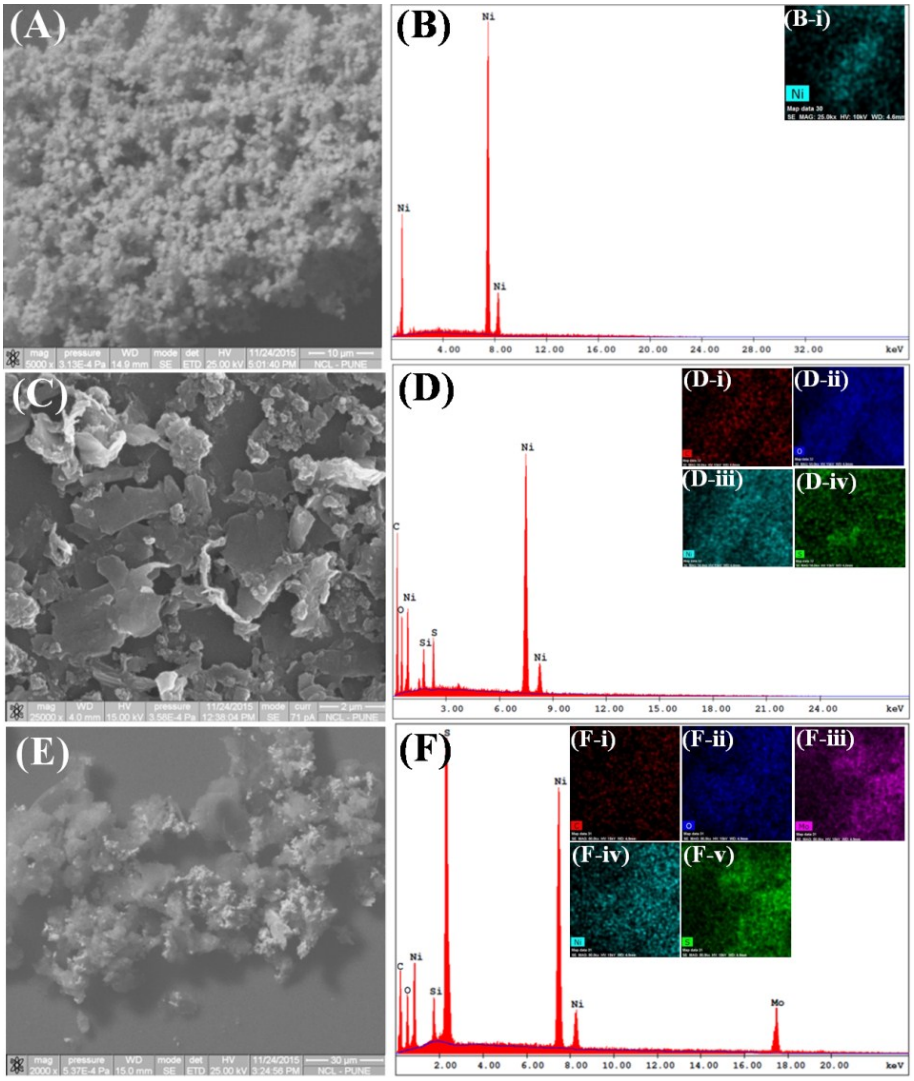

Figure S2. SEM micrograph of (A) Ni, (C) GrSC8Ni and (D) $GrMoS_2SC8Ni$ electrocatalyst; SEM-EDS, Inset with elemental mapping of (B) Ni, (D) GrSC8Ni and (F) $GrMoS_2SC8Ni$ electrocatalyst

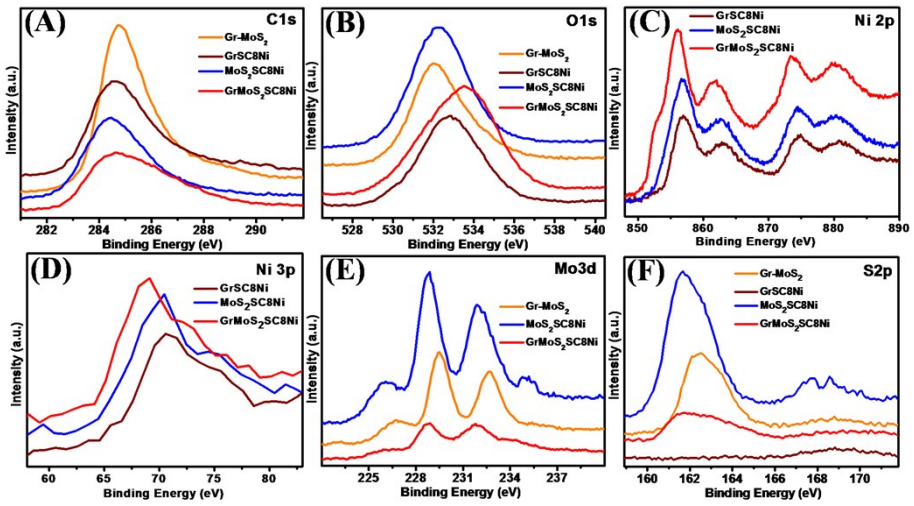

Figure S3. Comparative XPS spectra of (A) C1s, (B) O1s, (C) Ni 2p, (D) Ni 3p (E) Mo3d and (F) S2p spectra of Gr, MoS_2 and it´s respective composites.

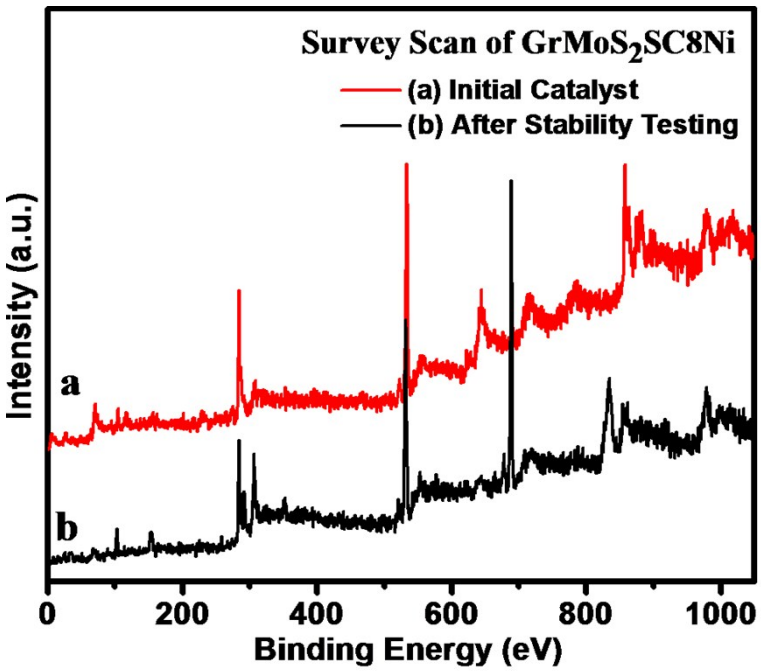

Figure S4. Comparative XPS survey scan of $GrMoS_2SC8Ni$ (a) Initial Catalyst and (b) After Stability Testing.

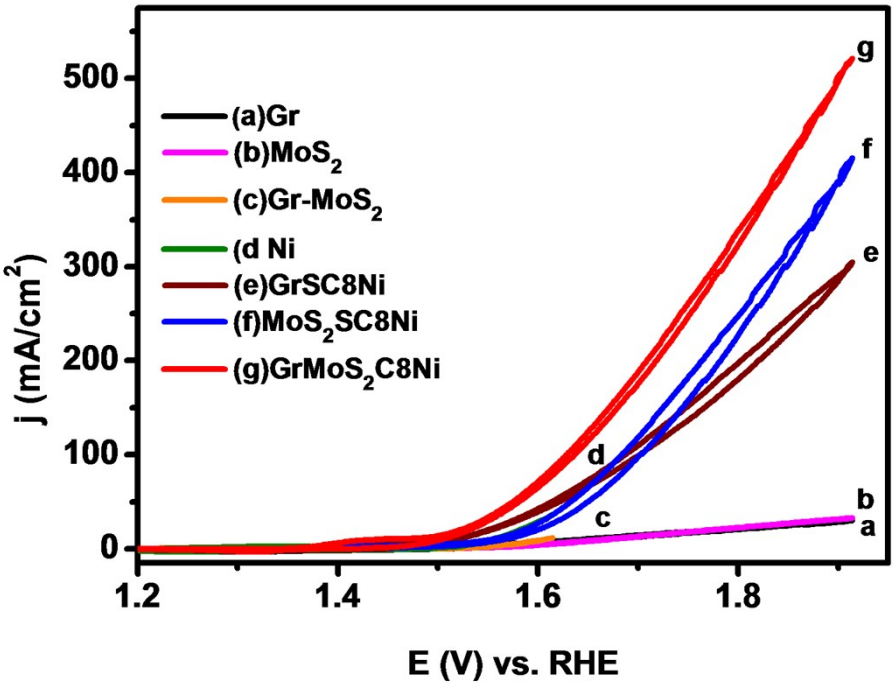

Figure S5. Comparative CV plots of (a)Gr (b) MoS_2, (c) Gr-MoS_2, (d) Ni, (e) GrSC8Ni, (f) MoS_2SC8Ni, and (g) $GrMoS_2SC8Ni$ electrocatalysts in 1 M KOH electrolytes.

Figure S5 shows the CVs of Ni and its composites obtained after different numbers of cycles. Figure S5(g) shows that the $GrMOS_2SC8Ni$ nanocomposite catalyst shows the oxidation wave attributed to the catalytic oxidation of water. With further cycling, the above oxidation/reduction waves increased in amplitude and

approached a stable value after 100 cycles, suggesting the activation of nanomaterial (i.e., Ni NPs) on the electrode surface.[1,2] Figure S5 (a, b, c and d) shows that the redox waves assignable to the Gr, MoS_2, Gr-MoS_2 and Ni respectively are all ill shaped. The OER catalytic current of it increases initially until reaching a maximum after 100 cycles and then drops quickly, indicative of poor catalyst stability. For GrSC8Ni, MoS_2SC8Ni and GrMoS_2SC8Ni nanocomposite material [Figure S5 (e, f and g)], the OER current decreases slightly during the first 100 cycles. However, this OER activity gradually decreases with CV cycling, consistent with previous reports that RuO_2 and IrO_2 suffer from large chemical degradation during OER process.[3] GrMoS_2SC8Ni nanocomposite material afford the largest oxygen-evolving current among the studied catalysts. Remarkably, the current density of 10 mA cm^{-2}, which is a metric relevant to solar fuel synthesis.[4] GrMoS_2SC8Ni nanocomposite material achieved at overpotential smaller than that GrSC8Ni, MoS_2SC8Ni catalysts, Ni and other precursor materials. (Figure S5 and Table S1 of ESI). By contrast, GrSC8Ni and MoS_2SC8Ni nanocomposite material and commercial Pt/C fail to reach such current density. During OER study first we perform a CV and then LSV study.

Table S1. OER performance of the reported Ni based catalyst.

Table S1: OER performances in the basic medium of present catalyst and other Nickel based electro catalyst.

Sr. No	Catalyst	Current Density (j)	Overpotential at (j)	Tafel slope ($mV\ dec^{-1}$)	Reference
1	Gr	10 mA/cm^2	528 mV	363 $mV\ dec^{-1}$	Current Work
2	MoS_2	10 mA/cm^2	436 mV	226 $mV\ dec^{-1}$	Current Work
3	Gr-MoS_2	10 mA/cm^2	343 mV	117 $mV\ dec^{-1}$	Current Work
4	Ni	10 mA/cm^2	325 mV	67 $mV\ dec^{-1}$	Current Work
5	GrSC8Ni	10 mA/cm^2	314 mV	51 $mV\ dec^{-1}$	Current Work
6	MoS_2SC8Ni	10 mA/cm^2	234 mV	48 $mV\ dec^{-1}$	Current Work
7	GrMoS_2SC8Ni	10 mA/cm^2	214 mV	31 $mV\ dec^{-1}$	Current Work
8	Amorphous $Ni(OH)_2$	10 mA/cm^2	344 mV	46 $mV\ dec^{-1}$	Cryst. Growth Des. 2015, 15, 4475-4483.
9	$Ni_{1-x}FexOOH$	10 mA/cm^2	~320 mV	50 $mV\ dec^{-1}$	J. Phys. Chem. C 2015, 119, 18303-18316.
10	$Ni_{0.69}Fe_{0.31}O_x$/C)	10 mA/cm^2	280 mV	30 $mV\ dec^{-1}$	Langmuir 2014, 30, 7893-7901.
11	NiCo LDH	10 mA/cm^2	367 mV	40 $mV\ dec^{-1}$	Nano Lett. 2015, 15, 1421-1427.
12	β-$Ni(OH)_2$ nanosheets	10 mA/cm^2	425 mV	60 $mV\ dec^{-1}$	Chem. Mater. 2015, 27, 5702-5711.
13	ALD NiS_x film	10 mA/cm^2	372 mV	56 $mV\ dec^{-1}$	Chem. Mater. 2016, 28, 1155-1164.
14	PNG-NiCo	5 mA/cm^2	373 mV	156 $mV\ dec^{-1}$	ACS NANO, 2013,11,10190-10196.
15	Ni-Co binary oxide	10 mA/cm^2	~325 mV	~39 $mV\ dec^{-1}$	ACS NANO, 2014,8,9518-9523.
16	rGO ($Ni_{2/3}Fe_{1/3}$-rGO)	10 mA/cm^2	210 mV	40 $mV\ dec^{-1}$	ACS NANO, 2015 ,9,177-1984.
17	$Fe_{0.1}Ni_{0.9}O$	10 mA/cm^2	297 mV	37 $mV\ dec^{-1}$	ACS NANO, 2015, 9, 5180-5188.
18	Ni_2P/Ni/NF	10 mA/cm^2	200 mV	72 $mV\ dec^{-1}$	ACS Catal. 2016, 6, 714-721.
19	$Ni_{1-x}Fe_x$/NC	10 mA/cm^2	330 mV	45 $mV\ dec^{-1}$	ACS Catal. 2016, 6, 580-588.
20	3D-OMNiSA	10 mA/cm^2	254 mV	39 $mV\ dec^{-1}$	ACS Catal. 2016, 6, 1446-1450.
21	Ni0.9Fe0.1Ox	10 mA/cm^2	336 mV	30 $mV\ dec^{-1}$	J. Am. Chem. Soc. 2012, 134, 17253-17261.
22	NiFe-LDH/CNT	10 mA/cm^2	300 mV	35 $mV\ dec^{-1}$	J. Am. Chem. Soc. 2013, 135, 8452-8455.
23	$Ni(OH)_2$/NiOOH	10 mA/cm^2	300 mV	40 $mV\ dec^{-1}$	J. Am. Chem. Soc. 2013, 135, 12329-12337.
24	α-$Ni(OH)_2$	10 mA/cm^2	331 mV	42 $mV\ dec^{-1}$	J. Am. Chem. Soc. 2014, 136, 7077-7084.
25	Ni3N nanosheets/CC	10 mA/cm^2	400 mV	45 $mV\ dec^{-1}$	J. Am. Chem. Soc. 2015, 137, 4119-4125.
26	Sandwich like NiFe/C	10 mA/cm^2	~210 mV	30 $mV\ dec^{-1}$	ACS Appl. Mater. Interfaces 2015, 7, 9203-9210.
27	[Ni,Fe]O	10 mA/cm^2	300 mV	~48 $mV\ dec^{-1}$	ACS Appl. Mater. Interfaces 2015, 7, 19755-19763.
28	NiS@SLS	11 mA/cm^2	297 mV	47 $mV\ dec^{-1}$	ACS Appl. Mater. Interfaces 2016, 8, 5509-5516.
29	MWCNTs@NCS-2	10 mA/cm^2	~440 mV	96 $mV\ dec^{-1}$	ACS Appl. Mater. Interfaces 2016, 8, 945-951.
30	$La(Co_{0.71}Ni_{0.25})0.96_{-\delta}$	10 mA/cm^2	265 mV	71 $mV\ dec^{-1}$	ACS Appl. Mater. Interfaces 2016, 8, 6019-6031.
31	$NiSe_2$/Ti	20 mA/cm^2	295 mV	82 $mV\ dec^{-1}$	ACS Appl. Mater. Interfaces 2016, 8, 4718-4723.
32	SL Ni(OH)2	5 mA/cm^2	302 mV	47 $mV\ dec^{-1}$	ACS Appl. Mater. Interfaces 2014, 6, 10172-10180.
33	CQD/NiFe-LDH	10 mA/cm^2	235 mV	35 $mV\ dec^{-1}$	ACS Appl. Mater. Interfaces 2014, 6, 7918-7925.
34	NiFeMn-LDH	20 mA/cm^2	~289 mV	~47$mV\ dec^{-1}$	*Chem. Commun.*, 2016, 52, 908-911.
35	NiFe LDH/oGSH,	10 mA/cm^2	350 mV	54 $mV\ dec^{-1}$	J. Mater. Chem. A, 2015,00, 1-7.
36	NiMo HNRs/TiM	10 mA/cm^2	310 mV	68 $mV\ dec^{-1}$	J. Mater. Chem. A, 2015, 3, 20056-20059.
37	NiFe LDH array	10 mA/cm^2	210 mV	31 $mV\ dec^{-1}$	J. Mater. Chem. A, 2016, 4, 167-172.

References:

1 Oliva, P.; Leonardi, J.; Laurent, J. F.; Delmas, C.; Braconnier, J. J.; Figlarz, M.; Fievet, F.; Deguibert, A. *J. Power Sources* 1982, 8, 229.

2 Medway, S. L.; Lucas, C. A.; Kowal, A.; Nichols, R. J.; Johnson, D. J. *Electroanal. Chem*. 2006, 587, 172.

3 Kinoshita, K. Electrochemical Oxygen Technology; *Wiley-Interscience: New York*, 1992.

4 Gorlin, Y.; Jaramillo, T. F. *J. Am. Chem. Soc*. 2010, 132, 13612.